Analysis of EXAFS Spectra of Crystalline Copper using Classical Anharmonic Correlated Einstein Model

Tong Sy Tien*

Institute of Research and Development, Duy Tan University, Da Nang 550000, Vietnam

Abstract: In this work, the temperature dependence of extended X-ray absorption fine structure (EXAFS) of the crystalline copper structure was calculated and analyzed using the anharmonic correlated Einstein model and the classical statistical theory. The thermodynamic parameters of a system are derived from an anharmonic effective potential that has taken into account the influence of all nearest neighbors of absorbing and backscattering atoms in the crystal lattice with thermal vibrations, where the Morse potential is assumed to characterize the interactions between each pair of atoms and the function of anharmonic EXAFS spectra presented in terms of the cumulant expansion up to the fourth-order. Analytical expressions for the first four cumulants and their contribution to amplitude reduction and phase shift obtained in the simple form of the mean-square relative displacement or the correlated Einstein frequency. The numerical results for crystalline copper were in good agreement with those obtained by the other theoretical procedures and experiments at several temperatures. The analytical results show that this calculation model is useful to reduce measurement and data analysis of experimental EXAFS spectra.

Keywords: EXAFS spectra, crystalline copper, anharmonic correlated Einstein model, classical statistical theory.

1. INTRODUCTION

The extended X-ray absorption fine structure (EXAFS) has been developed into a powerful technique and is widely used to determine many structural parameters and dynamic properties of materials [1-5]. In the case of harmonic oscillators, a reduction factor of the EXAFS amplitude is multiplied, which is so-called a Debye-Waller factor (DWF) and is arisen as a natural consequence of fluctuations in interatomic distances and are easily added by the average of $\left\langle e^{2ikR} \right\rangle$ over many paths [6,7]. However, the position of atoms is not stationary, and their interatomic distance always changes due to thermal vibrations [4-6]. The sensitivity of EXAFS oscillations to these thermal vibrations was detected by Beni and Platzman (1976) [2] and discussed detail by Eisenberger and Brown (1979) [3]. They cause thermal disorder and anharmonic effects on crystal vibrations and will smear out the EXAFS oscillations [3,6]. Therefore, in the case of anharmonic oscillators, an account of DWF for displacement-displacement correlation function with the local disorder is especially crucial for achieving the correct EXAFS amplitudes, while an account of the anharmonicity is essential for a proper understanding of the EXAFS phase [7-8]. The sensitivity of EXAFS oscillations to anharmonic effects and its capability to give unique information about anharmonic interactions, which were reviewed by Tranquada and Ingalls (1983) [9] and Crozier *et al*. (1988) [10], are being effectively applied to investigate the structure and dynamic parameters of disordered systems [11-16].

In a solid exhibiting local dynamic disorder of the atomic positions of a single shell around a central atom described through the radial pair distribution-function (RDF) [3-6], and the cumulants of this function (or cumulants) were determined to be more stable and interpreted more naturally by Kubo (1962) [17]. The use of cumulants to investigate local disorder of the EXAFS spectra was introduced by Rehr (1979) [8,18] who showed that the DWF is generally complex and has a natural cumulant expansion in powers of the photoelectron wavenumber. The EXAFS function was described in detail via the cumulant expansion approach (ratio method) by Bunker (1983) [7] and exploited by Tranquada and Ingalls (1983) [9]. The ratio method is particularly appealing because it summarizes the relevant structural and dynamic information in a few parameters that are easily obtained from the experimental EXAFS spectra [9,10,19-22]. The amplitude and phase of the anharmonic EXAFS spectra are expanded as a series of cumulants of the interatomic distance distribution, which is effectively achieved in analyzing experimental EXAFS spectra [9-10,19]. The importance of including higher-order cumulants in the anharmonic EXAFS analysis has been recognized in many works [23-27].

Many theoretical approaches have been used to calculate and evaluate the contribution of thermal vibrations to the anharmonic EXAFS spectra. For quantum approaches, several methods have been proposed such as the full lattice dynamic (FLD) approach, path-integral effective-potential (PIEP)

*Address correspondence to this author at the Institute of Research and Development, Duy Tan University, Da Nang 550000, Vietnam; Tel: +84912439564; Fax: +8435537511; E-mail: tongsytien@duytan.edu.vn

E-ISSN: 2410-4701/19

method, equation of motion (EM) method, path-integral Monte Carlo (PIMC) calculation, density functional theory (DFT) calculations, and anharmonic correlated Debye (ACD) model, which were described by Miyanaga and Fujikawa (1994b) [28], Yokoyama (1998,1999) [29,30], Poiarkova and Rehr (1999) [31], Beccara *et al.* (2003,2008) [32,33], Vila *et al*. (2007,2012) [34,35], Hung *et al*. (2010) [36], respectively. These quantum approaches took into account the quantum effects at low temperatures and the anharmonic effects at high temperatures. However, they still have a limitation in which the results of the EXAFS cumulants are not expressed in explicit forms. This limitation leads to the analysis of the anharmonic EXAFS spectra to determine thermodynamic parameters that are quite complicated because it needs to perform many computational steps with various parameters. For the classical approach, using a classical approximation based on the force constants of an effective potential was proposed by Stern *et al*. (1991) [37], where the parameters of the interatomic potential of the system were unknown. It can calculate the temperature dependence of EXAFS cumulants up to the fourth-order and obtain simple results. This classical approach works well at high temperatures and was used effectively for analyzing anharmonic EXAFS spectra of some crystals and metals at high temperatures [22,38-40].

Additionally, for two-atom systems, EXAFS cumulants can be expressed as a function of the force constant of a one-dimensional bare interaction potential [18,19,41], while for many-atom systems, EXAFS cumulants are often connected to the force constants of a one-dimensional effective pair potential by analytical expressions similar to those for two-atom systems [18,42]. However, the connection between the EXAFS cumulants and the thermodynamic parameters of many-atom systems remains a matter of great interest [8,18,42], especially regarding the meaning of effective potential [43,44]. The sensitivity of the EXAFS cumulants with the nature of the bonding potential of atoms was suggested by Rehr *et al*. (1995) [45]. Hung and Rehr (1997) [18] then introduced a calculated model for the anharmonic effective potential based on the correlated Einstein model [46] and the contribution of the anharmonic effects that take into account the interaction of absorbing and backscattering atoms with their nearest neighbors and it called the anharmonic correlated Einstein (ACE) model.

Recently, for the ACE model using the quantum statistical theory (henceforth cited as the QACE model), it was successfully applied to calculate and evaluate the EXAFS spectra for various types of crystal lattices by Hung *et al*. (2017,2019) [13-14,15], Fornasini *et al*. (2017) [16], Duc *et al*. (2019) [47], and Vuong *et al.* (2019) [48]. For the ACE model [18] using the classical statistical theory [37] (henceforth cited as the CACE model), it was efficiently applied to calculate and analyze the EXAFS spectra for crystalline zinc (Zn) & cadmium (Cd) by Hung *et al*. (2014) [43] and crystalline germanium (Ge) by Tien *et al.* (2019) [44]. However, the QACE model only extends the EXAFS cumulants up to the third-order, and the CACE model only calculates for the hexagonal close-packed crystals and diamond crystals, while the experimental EXAFS spectra were analyzed for crystalline copper using the cumulant expansion approach up to the fourth-order [38,49]. Therefore, the application and development of a CACE model to efficiently calculate and analyze the anharmonic EXAFS spectra of Cu will be a necessary addition to the analysis of EXAFS technique.

The purpose of this work is to develop a more suitable calculation-model for analysis of the anharmonic EXAFS spectra of the first coordination shell of crystalline copper(Cu) based on the CACE model. In this work, the analytical expressions for the anharmonic effective potential and local force constants are derived from the structure of a small cluster of immediate neighboring atoms around the absorbing and backscattering atoms, where the anharmonic effective potential is expanded up to the fourth-order instead of lower orders, and the Morse potential characterizes the interaction between a pair of atoms. The dependence of the first four EXAFS cumulants and the EXAFS amplitude and phase is calculated and described in the simple form of the mean-square relative displacement or the correlated Einstein frequency. Our numerical results for Cu are found to be in good agreement with those obtained by the QACE model [14], the ACD model [36], and experiments [14,38,49] at various temperatures. From the analysis of the comparison results, we discuss advances in studies on evaluating the role and meaning of the EXAFS cumulants in the analysis of the temperature dependence of the EXAFS amplitude and phase.

This article is organized as follows. The theoretical model and basic formulae of the EXAFS oscillation function are introduced in Sec. 2. Sec. 3 calculates the anharmonic effective potential and the first four cumulants of EXAFS spectra of face-centered cubic crystals are calculated on the basis of the CACE model. The numerical results for Cu compared with

those other theoretical procedures and experiments are discussed in Sec. 4. Sec. 5 concludes on the present investigation.

2. BASIC FORMULAE OF THE EXAFS FUNCTION

The thermal average of the EXAFS oscillation function of a single coordination shell has the form [6,7,19,20]:

$$\chi(k) = A(k)\sin\Phi(k), \tag{1}$$

where $A(k)$ and $\Phi(k)$ are the EXAFS amplitude and phase, respectively, and k is the photoelectron wavenumber.

For the distribution of identical atoms and including non-Gaussian disorder, the *K*-edge EXAFS oscillation is described within the framework of single-scattering and plane-wave approximations by [7,9,10]

$$\chi(k) = \frac{NS_0^2(k)}{k} F(k)\, Im\left\{\left\langle \frac{e^{-2r/\lambda}}{r^2} \mathrm{e}^{2ikr} \right\rangle e^{i\delta(k)}\right\}, \tag{2}$$

where λ is the electron mean free path, N is the coordination number, $F(k)$ is the atomic backscattering amplitude, $\delta(k)$ is the net phase shift, the angular brackets $\langle\ \rangle$ are the thermal average, $S_0^2(k)$ is an amplitude reduction factor due to the many-body effects, and r is the instantaneous distance between the absorber atom and one neighboring atom.

The temperature dependence of the normalized *K*-edge EXAFS oscillations $k^2\chi(k)$ of Cu is shown in Figure **1**. It can be seen that the amplitude attenuation and phase shift to the right as the temperature *T* increases, which indicates that the anharmonic effects caused by thermal vibrations significantly influence the EXAFS oscillations.

The cumulant expansion approach in powers of k in the form of a Taylor series is often used [7,8,10]:

$$\left\langle \mathrm{e}^{2ikr} \right\rangle = \exp\left\{2ikr_0 + \sum_n \frac{(2ik)^n}{n!}\sigma^{(n)}\right\}, \tag{3}$$

where the coefficients $\sigma^{(n)}$ are cumulants, r_0 is the equilibrium distance between the absorbing and backscattering atoms, the even-order cumulants contribute primarily to the amplitude, and the odd-order cumulants contribute primarily to the phase of the anharmonic EXAFS spectra.

The analysis of the temperature dependence of the EXAFS spectra involves the cumulants that are expressed in terms of the power moments of the radial pair distribution-function (RDF). The first four EXAFS cumulants (with respect to the mean) are given by [8,10,19,50]

$$\sigma^{(1)} = \langle r \rangle - r_0, \tag{4}$$

$$\sigma^{(2)} \equiv \sigma^2 = \left\langle (r-R)^2 \right\rangle, \tag{5}$$

$$\sigma^{(3)} = \left\langle (r-R)^3 \right\rangle, \tag{6}$$

$$\sigma^{(4)} = \left\langle (r-R)^4 \right\rangle - 3(\sigma^2)^2, \tag{7}$$

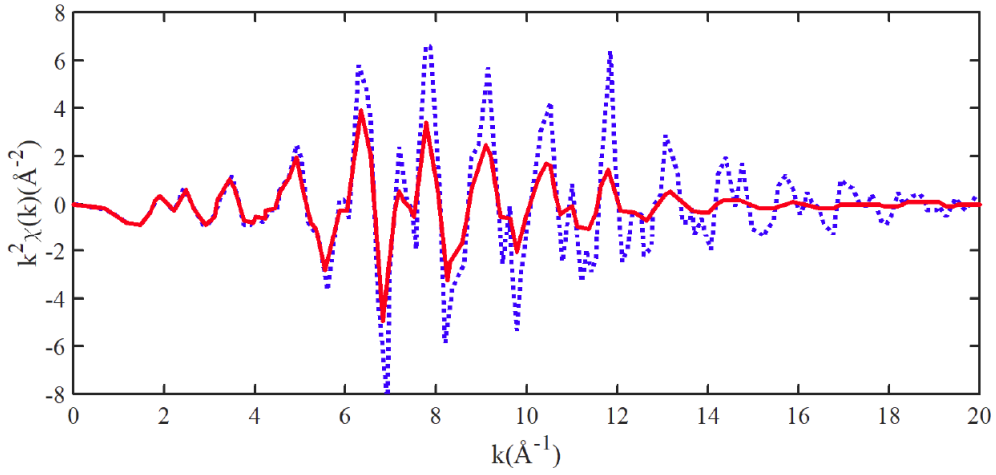

Figure 1: The normalized *K*-edge EXAFS oscillations $k^2\chi(k)$ of Cu at 300 K (dotted blue line) and 500 K (solid red line) [49].

where the second cumulant σ^2 is the parallel mean square relative displacement (MSRD) of the effective path length associated with a given multiple-scattering (MS) path, and the average distance between central and backscattering atom is $R = \langle r \rangle = \frac{1}{N}\int_0^\infty \rho(T,r) r\, dr$ with $\rho(T,r)$ is true RDF [19].

Using the cumulant expansion approach in Eq. (3) and expanding the asymmetric terms in the brackets of Eq. (2) in a Taylor series about R and rewrites the thermal average in terms of cumulants [19,51], if the small-term yields from the mean free path (which implies a complex *k*) are neglected and approximated to the fourth cumulant, the result can be obtained as

$$\left\langle \frac{e^{-2r/\lambda}}{r^2} e^{2ikr} \right\rangle \approx \frac{e^{-2R/\lambda}}{R^2} \exp\left\{ \begin{array}{l} 2ikr_0 + 2k\sigma^{(1)} - 2k^2\sigma^2 - 4ik\sigma^2 \\ \left(\frac{1}{R} + \frac{1}{\lambda}\right) - \frac{4i}{3}k^3\sigma^{(3)} + \frac{2}{3}k^4\sigma^{(4)} \end{array} \right\}. \quad (8)$$

Replacing Eq. (8) into Eq. (2), we obtain the formalism of the *K*-edge EXAFS function based on the cumulant expansion, including the anharmonic effects as

$$\chi(k) \cong \frac{NS_0^2(k)e^{-2R/\lambda}}{kR^2} F(k) \exp\left\{-2k^2\sigma^2 + \frac{2k^4}{3}\sigma^{(4)}\right\} \sin\left\{2kr_0 + 2k\sigma^{(1)} - 4k\sigma^2\left(\frac{1}{R} + \frac{1}{\lambda}\right) - \frac{4k^3}{3}\sigma^{(3)} + \delta(k)\right\}. \quad (9)$$

Thus, anharmonicity in the potential yields additional terms in the amplitude and phase of the anharmonic EXAFS spectra [3,5,8], which if ignored can lead to non-negligible errors in the structural parameters [5-10,18].

Inferring from Eq. (9), the temperature *T* and wavenumber *k* dependence of the $A(k,T)$ and phase $\Phi(k,T)$ is expressed as

$$A(k,T) = \frac{NS_0^2(k)e^{-2R(T)/\lambda(k)}}{kR^2(T)} F(k) \times \exp\left\{-2k^2\sigma^2(T) + \frac{2k^4}{3}\sigma^{(4)}(T)\right\}, \quad (10)$$

$$\Phi(k,T) = 2kr_0 + 2k\sigma^{(1)}(T) - 4k\sigma^2(T) \left\{\frac{1}{R(T)} + \frac{1}{\lambda(k)}\right\} - \frac{4k^3}{3}\sigma^{(3)}(T) + \delta(k). \quad (11)$$

Assuming the quantities $F(k), \delta(k), S_0^2(k)$, and $\lambda(k)$ to be the same at temperatures T_1 and T_2 [19,22,52-53], we deduce the logarithm of the amplitude ratio $M(k,T_1,T_2) = \ln\left[A(k,T_2)/A(k,T_1)\right]$ and the linear phase difference $\Delta\Phi(k,T_1,T_2) = \Phi(k,T_2) - \Phi(k,T_1)$ between temperatures T_2 and T_1 from Eqs. (10) and (11) as follows:

$$M(k,T_1,T_2) \simeq -2k^2\left\{\sigma^2(T_2) - \sigma^2(T_1)\right\} + \frac{2k^4}{3}\left\{\sigma^{(4)}(T_2) - \sigma^{(4)}(T_1)\right\}, \quad (12)$$

$$\Delta\Phi(k,T_1,T_2) \simeq 2k\left\{\sigma^{(1)}(T_2) - \sigma^{(1)}(T_1)\right\} - 4k\left\{\frac{1}{r_0} + \frac{1}{\lambda}\right\}\left\{\sigma^2(T_2) - \sigma^2(T_1)\right\} - \frac{4k^3}{3}\left\{\sigma^{(3)}(T_2) - \sigma^{(3)}(T_1)\right\}. \quad (13)$$

Here, the term $-2\left\{\left[R(T_2) - R(T_1)\right]/\lambda(k) + \ln\left[R(T_2)/R(T_1)\right]\right\}$ is neglected in Eq. (12) because it is very small compared to the other terms in this equation, while the calculations of Eq. (13) deduced from Eq. (11) can use approximation $1/R(T) \simeq 1/r_0$ assuming $\sigma^{(1)} \ll r_0$ and $R(T) = r_0 + \sigma^{(1)}$ are derived from Eq. (3).

Thus, we can analyze anharmonic EXAFS spectra based on the temperature dependence of the first four cumulants to determine many structural parameters and dynamic properties of materials.

3. MODEL OF CALCULATING THE EXAFS CUMULANTS

3.1. Anharmonic Effective Potential in the ACE Model

To determine the thermodynamic parameters of a system, it is necessary to specify its anharmonic effective potential and force constants [12,18,43,44]. One considers a monatomic system with an anharmonic effective potential (ignored the constant contribution) is extended up to the fourth-order:

$$V_{eff}(x) = \frac{1}{2}k_0x^2 - k_3x^3 + k_4x^4, \quad (14)$$

where $x = r - r_0$ is the deviation of the interatomic distance from the potential minimum position, k_0 is the effective force constant, k_3 and k_4 are local force constants giving asymmetry of potential due to the inclusion of anharmonicity.

The Morse potential is assumed to describe the interatomic interaction model for the potential energy of a diatomic molecule [54], which is given in terms of the function by

$$V(x) = D\left(e^{-2\alpha x} - 2e^{-\alpha x}\right), \tag{15}$$

where x is the same previously defined value, α describes the width of the potential, and D is the dissociation energy.

Applying the Morse potential to calculate the interaction energy between each pair of atoms in cubic metals was proposed by Girifalco and Weizer (1959) [55]. In the present study, we expand the Morse potential to the fourth-order:

$$V(x) \cong -D + D\alpha^2 x^2 - D\alpha^3 x^3 + \frac{7}{12} D\alpha^4 x^4 . \tag{16}$$

In the relative vibrations of absorbing (A) and backscattering (B) atoms, including the effect of correlation and taking into account only the nearest-neighbor interactions, the anharmonic effective potential in the ACE model [18] is given by

$$V_{eff} = V(x) + \sum_{i=A,B} \sum_{j \neq A,B} V\left(\frac{\mu}{M_i} x \hat{R}_{AB} \hat{R}_{ij}\right), \tag{17}$$

where $\mu = M_A M_B / \left(M_A + M_B\right)$ is the reduced mass of the absorber and backscatterer with masses M_A and M_B, respectively, $\hat{R}$ is a unit vector, the sum i is the over absorbers ($i = A$) and backscatterers ($i = B$), and the sum j is over the nearest neighbors.

As can be seen on the right side of Eq. (17), the first term on the right concerns only the pair interaction potential of the absorbing and backscattering atoms and the second one describes the contribution of their nearest-neighbor atoms to the pair interaction potential and depends on the crystal structure type.

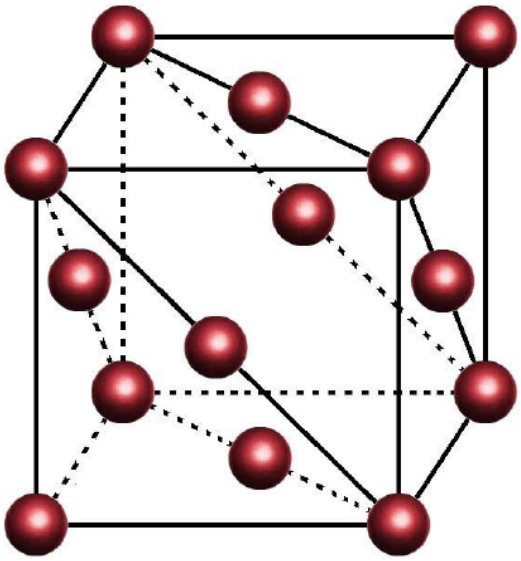

Figure 2: Model of the crystalline copper.

The model of the FCC structure of Cu is illustrated in Figure **2**. Applying Eq. (17) to this structure, the anharmonic effective potential is written as

$$V_{eff}(x) = V(x) + 4V(0) + 2V\left(-\frac{1}{2}x\right) + 8V\left(-\frac{1}{4}x\right) + 8V\left(\frac{1}{4}x\right) . \tag{18}$$

Using the Morse potential in Eq. (16) to calculate the anharmonic effective potential according to Eq. (18) and ignoring the overall constant, we obtain the result as

$$V_{eff}(x) = \frac{5}{2} D\alpha^2 x^2 - \frac{5}{4} D\alpha^3 x^3 + \frac{133}{192} \alpha^4 x^4 . \tag{19}$$

Comparing Eq. (14) with Eq. (19), we deduce the local force constants k_0, k_3, and k_4 as follows:

$$k_0 = 5D\alpha^2, \quad k_3 = \frac{5}{4} D\alpha^3, \quad k_4 = \frac{133}{192} D\alpha^4 . \tag{20}$$

The thermal vibration of atoms is characterized by the correlated Einstein frequency ω_E and temperature θ_E, which are calculated from the effective force constant k_0 in the following forms:

$$\omega_E = \sqrt{\frac{k_{eff}}{\mu}} = \sqrt{\frac{14D\alpha^2}{3m}}, \; \theta_E = \frac{\hbar \omega_E}{k_B} , \tag{21}$$

where k_B is the Boltzmann constant, $\hbar$ is the reduced Planck constant, and the masses of all atoms in the monatomic crystals are the same; that is, the mass of the atoms is $M_1 = M_2 = m$, so the reduced mass is $\mu = m/2$.

Consequently, the correlated Einstein frequency ω_E and temperature θ_E, and the force constants k_0, k_3, and k_4 are expressed in terms of the Morse potential parameters.

3.2. Temperature Dependence of EXAFS Cumulants within a Classical Statistical Theory

Using the effective anharmonic potential in Eq. (14) in the classical statistical limit and assuming that anharmonicity can be treated as a small perturbation, we determine the temperature dependence of the moments about the mean $\langle x \rangle$ by evaluating the thermal average in the third-order approximation [37]:

$$\left\langle x^n \right\rangle = \frac{\int_{-\infty}^{\infty} x^n \exp\left[-\frac{V_{eff}(x)}{k_B T}\right] dx}{\int_{-\infty}^{\infty} \exp\left[-\frac{V_{eff}(x)}{k_B T}\right] dx} \approx \frac{\int_{-\infty}^{\infty} x^n \exp\left[\frac{-k_{eff} x^2}{2k_B T}\right]\left[\sum_{n=0}^{3} \frac{1}{n!}\left(\frac{k_3 x^3 - k_4 x^4}{k_B T}\right)^n\right] dx}{\left(\frac{2\pi k_B T}{k_{eff}}\right)^{1/2}\left[1 + \frac{3(k_B T)}{k_{eff}^2}\left(\frac{5k_3^2}{2k_{eff}} - k_4\right)\right]}. \quad (22)$$

To obtain the temperature dependence of the first four EXAFS cumulants from Eqs. (4)–(7), we use Eq. (21) to calculate the moments $\left\langle x^n \right\rangle$ (n = 1, 2, 3, and 4) according to Eqs. (22), the analytical expressions are obtained in the lowest-orders as

$$\sigma^{(1)} = \langle x \rangle \simeq \frac{3k_B T}{20D\alpha}\left(1 - \frac{389k_B T}{1200D}\right); \quad (23)$$

$$\sigma^{(2)} = \left\langle \left(x - \langle x \rangle\right)^2 \right\rangle = \left\langle x^2 \right\rangle - \langle x \rangle^2 \simeq \frac{k_B T}{5D\alpha^2}\left(1 + \frac{47k_B T}{400D}\right); \quad (24)$$

$$\sigma^{(3)} = \left\langle \left(x - \langle x \rangle\right)^3 \right\rangle = \left\langle x^3 \right\rangle - 3\left\langle x^2 \right\rangle \langle x \rangle + 2\langle x \rangle^3 \simeq \frac{3(k_B T)^2}{50D^2\alpha^3}\left(1 - \frac{211k_B T}{400D}\right); \quad (25)$$

$$\sigma^{(4)} = \left\langle \left(x - \langle x \rangle\right)^4 \right\rangle - 3\left(\sigma^2\right)^2 = \left\langle x^4 \right\rangle + 12\left\langle x^2 \right\rangle \langle x \rangle^2 - 3\left\langle x^2 \right\rangle^2 - 4\left\langle x^3 \right\rangle \langle x \rangle - 6\langle x \rangle^4 \simeq \frac{137(k_B T)^3}{5000D^3\alpha^4}\left(1 + \frac{50649k_B T}{54800D}\right). \quad (26)$$

The truncation of the series in Eq. (22) serves as a convergence cutoff while including enough terms to accurately obtain the second lowest-order expressions for the moments. Because $k_B T / D << 1$, the respective expressions are obtained from Eqs. (23)–(26) in the lowest order as

$$\sigma^{(1)} \approx \frac{3k_B T}{20D\alpha} = \frac{3\alpha}{4}\sigma^2; \quad (27)$$

$$\sigma^{(2)} \approx \frac{k_B T}{5D\alpha^2} \equiv \sigma^2; \quad (28)$$

$$\sigma^{(3)} \approx \frac{3(k_B T)^2}{50D^2\alpha^3} = \frac{3\alpha}{2}\left(\sigma^2\right)^2; \quad (29)$$

$$\sigma^{(4)} \approx \frac{137(k_B T)^3}{5000D^3\alpha^4} = \frac{137\alpha^2}{40}\left(\sigma^2\right)^3. \quad (30)$$

Thus, as can be seen from Eqs. (27)–(30), the temperature dependence of the cumulants $\sigma^{(1)}$ and σ^2, $\sigma^{(3)}$, and $\sigma^{(4)}$ is proportional to T, T^2, and T^3, respectively. These results are similar to those obtained using the first-order thermodynamic perturbation theory [18] and the anharmonic correlated Debye model [36] at high temperatures. Moreover, the analytical expressions the first four EXAFS cumulants have been presented in the simple form of the cumulant σ^2 or MSRD.

4. NUMERICAL RESULTS AND DISCUSSION

To discuss the development and effectiveness of the CACE model for the analysis of EXAFS spectra in this work, we apply the formulae in Sec. 2 and the analytical expressions in Sec. 3 to the numerical calculations for Cu. Firstly, we calculate the temperature dependence of the first four EXAFS cumulants in the range from 0 K to 700 K. Our results are compared with those obtained using the QACE model [14], and the ACD model [36] based on the many-body perturbation approach and dispersion effect proposed by Hung *et al*. (2010) [36]. Our results are also compared with the experimental values obtained via the EXAFS spectrometer using the determining anharmonic pair potential parameters to the classical approach performed by Pirog *et al*. (2002) [38] at the Synchrotron Radiation Siberian Center (SSRC), Russia, from the EXAFS measurements using the best-fitting to ratio method obtained by Fornasini *et al.* (2004) [49] at the Beamline BM08, European Synchrotron Radiation Facility (ESRF), France, and from the EXAFS data measured at the Beamline BL8, Synchrotron Light Research Institute (SLRI), Thailand by Hung *et al.* (2017) [14]. In these comparisons, the results calculated using the QACE model [14] and the ACD model [36] are in the range from 0 K to 700 K. The experimental values are at 300 K, 400 K, and 500 K [14], at 6 different temperatures between 293 K and 573 K [38], and at 19 different temperatures between 4 K and 500 K [49], respectively. Then, we analyze the logarithm of amplitude ratio and the phase difference of the anharmonic EXAFS spectra at 300 K and 500K in the wavenumber range from 0 $Å^{-1}$ to 20 $Å^{-1}$. Our results are compared with those obtained using the filtered EXAFS signal obtained using the ratio method suggested by Fornasini *et al.* (2004) [49] in the wavenumber range from approximately 3 $Å^{-1}$ to 14 $Å^{-1}$.

Table 1: The Thermodynamic Parameters k_0, k_3, k_4, ω_E, and θ_E of Cu Obtained using the CACE Model, the QACE Model [14] and other Experiments [38,49]

Method	k_0 (eVÅ^{-2})	k_3 (eVÅ^{-3})	k_4 (eVÅ^{-4})	ω_E ($\times 10^{13}$Hz)	θ_E (K)
CACE model[a]	3.17	1.08	0.83	3.10	236.8
QACE model[b]	3.17	1.08		3.10	236.8
Experiment[c]	3.20	1.30	1.40	3.12	238.1
Experiment[d]	3.20	1.37	1.46	3.12	231.9

[a]This work.
[b]Reference [14].
[c]Reference [38].
[d]Reference [49].

Lastly, from these comparisons, we evaluate and comment on the results calculated via the CACE model in this work.

The thermodynamic parameters k_0, k_3, k_4, ω_E, and θ_E for Cu are calculated by Eqs. (20) and (21) and given in Table **1**, where the Morse potential parameters $D = 0.3429$ eV and $\alpha = 1.3588$ Å^{-1} derived from experimental values of the energy of vaporization. Our results are compared with those obtained using the QACE model [14] and other experiments [38,49]. The correlated Einstein frequency ω_E and temperature θ_E in Refs. [14, 38] are deduced from the effective force constant k_0, and the correlated Einstein temperature θ_E in Ref. [49] is obtained using the correlated Debye temperature $\theta_D = \sqrt{2}\,\theta_E$ [18,36]. As can be seen from Table **1**, the comparisons show no significant difference, especially for the effective force constant k_0, correlated Einstein frequency ω_E, and temperature θ_E.

Figure **3** shows the temperature dependence of (a) the first cumulant $\sigma^{(1)}(T)$ and (b) the second cumulant $\sigma^2(T)$ of Cu is calculated using Eqs. (27) and (28), respectively. At temperatures above $\theta_E \approx 237$ K, our results calculated using the CACE model indicate good agreement with those obtained using the QACE model [14] and the ACD model [36], and with the experimental values of Refs. [14, 38, 49] (only for the second cumulant) as seen in Figure **3**, in which the experimental values of Ref. [38] for the first cumulant are derived from the experimental interaction-distance $R(T)$ according to Eq. (4). At 300 K, the results obtained using the CACE model, the QACE model the ACD model, are $\sigma^{(1)} \simeq 8.4\times10^{-3}$ Å and $\sigma^2 \simeq 8.3\times10^{-3}$ Å^2, $\sigma^{(1)} \simeq 8.8\times10^{-3}$ Å and $\sigma^2 \simeq 8.7\times10^{-3}$ Å^2 [14], and $\sigma^{(1)} \simeq 8.4\times10^{-3}$ Å and $\sigma^2 \simeq 8.6\times10^{-3}$ Å^2 [36], respectively, while the experimental values are $\sigma^{(1)} \approx 8.7\times10^{-3}$ Å and $\sigma^2 \approx 8.4\times10^{-3}$ Å^2 [14], and $\sigma^2 \approx 8.4\times10^{-3}$ Å^2 [49] at 300 K, and $\sigma^{(1)} \approx 8.9\times10^{-3}$ Å and $\sigma^2 \approx 6.8\times10^{-3}$ Å^2 at 293 K [38].

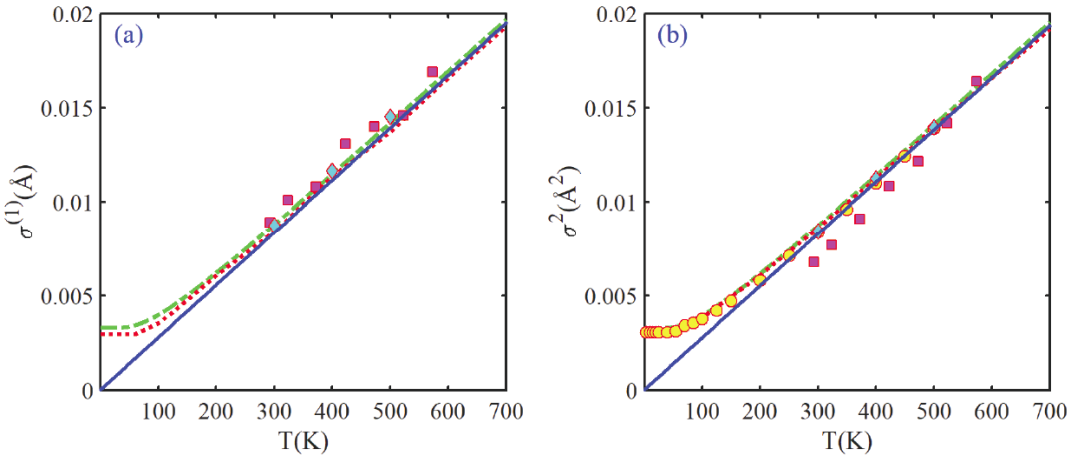

Figure 3: Temperature dependence of the first (**a**) and second (**b**) cumulants of Cu obtained using the CACE model (solid blue lines), the QACE [14] (dashed-dotted green lines), the ACD model [36] (dotted red lines), and other experiments from Refs. [14] (full cyan diamonds), [38] (full magenta squares), and [49] (full yellow circles).

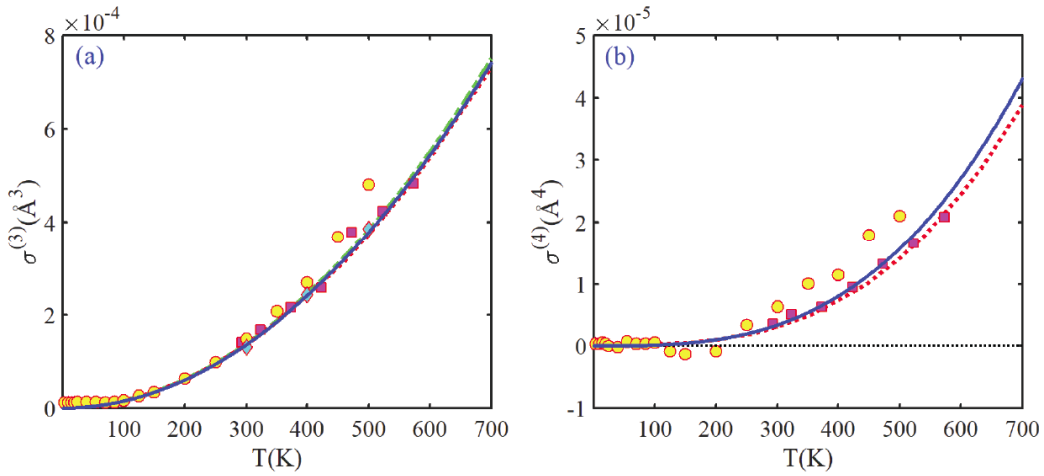

Figure 4: Temperature dependence of the third (a) and fourth (b) cumulants of Cu obtained using the CACE model (solid blue lines), the QACE [14] (dashed-dotted green line), the ACD model [36] (dotted red lines), and other experiments from Refs. [14] (full cyan diamonds), [38] (full magenta squares), and [49] (full yellow circles).

Figure **4** shows the temperature dependence of (a) the third cumulant $\sigma^{(3)}(T)$ and (b) the fourth cumulant $\sigma^{(4)}(T)$ of Cu is calculated using Eqs. (29) and (30), respectively. Our results calculated using the CACE model indicate good agreement with those obtained using the ACD model [36], and the QACE model [14] (only for the third cumulant), and with the experimental values of Refs. [14, 38, 49] (only for the third cumulant) as seen in Figure **4**, especially at temperatures not too low (the applicable limits for the third and fourth cumulants in the low-temperature range have been discussed in detail in Ref. [44]). At 300 K, the results obtained using the CACE model, the QACE model, and the ACD model are $\sigma^{(3)} \simeq 1.4\times10^{-4}$ Å^3 and $\sigma^{(4)} \simeq 3.4\times10^{-6}$ Å^4, $\sigma^{(3)} \simeq 1.4\times10^{-4}$ Å^3 and $\sigma^{(4)} \simeq 4.3\times10^{-6}$ Å^4 [14], $\sigma^{(3)} \simeq 1.4\times10^{-4}$ Å^3 and $\sigma^{(4)} \simeq 3.2\times10^{-6}$ Å^4 [36], respectively, while the experimental values are $\sigma^{(3)} \approx 1.3\times10^{-4}$ Å^3 [14], and $\sigma^{(3)} \approx 1.5\times10^{-4}$ Å^3 and $\sigma^{(4)} \approx 6.3\times10^{-6}$ Å^4 [49] at 300 K, and $\sigma^{(3)} \approx 1.4\times10^{-4}$ Å^3 and $\sigma^{(4)} \approx 3.6\times10^{-6}$ Å^4 at 293 K [38]. As can be seen from Refs. [14, 36], our results for first three cumulants are the same as the corresponding results calculated by the QACE model [14] and ACD model [36] in the high-temperature limit, while our result for the fourth cumulant is slightly greater than the result calculated by the ACD model [36] (the QACE model [14] can only calculate cumulants up to the third-order). Here, the local force constants in the results of Refs. [14, 36] are replaced by terms of the Morse potential parameters from Eq. (20).

Thus, the results of the temperature dependence of the first four EXAFS cumulants calculated using the present CACE model satisfied all of their fundamental properties compared to other theoretical models and experiments at temperatures above the correlated Einstein temperature, which is explained because anharmonicity in EXAFS spectra appears from about room temperature. These results described the influence of anharmonic effects on the classical limit via thermal vibration-contributions at high temperatures.

Figure **5** shows the wavenumber dependence of (a) logarithm of the amplitude ratio $M(k) = \ln\left[A(k,500\,K)/A(k,300\,K)\right]$ and (b) the phase difference $\Delta\Phi(k) = \Phi(k,500\,K) - \Phi(k,300\,K)$ of Cu is calculated using Eqs. (12) and (13), respectively. It can be seen that our results calculated using the CACE model indicate good agreement with those obtained via the ratio method [49] in the wavenumber range from approximately 3 Å^{-1} to 14 Å^{-1}. At $k = 14$ Å^{-1} and our results are $M \simeq -1.86$ and $\Delta\Phi \simeq -0.89$ rad, while the results obtained using the ratio method are $M \simeq -1.84$ and $\Delta\Phi \simeq -1.06$ rad [49]. The logarithm of the amplitude ratio $M(k)$, including the contributions of the terms that contain the second cumulant (henceforth denoted as $M_1(k)$) and fourth cumulant (henceforth denoted as $M_2(k)$) as seen via Eq. (12). As can be seen from Figure **5a**, our calculated result demonstrates that $M_1(k)$ is the major contributor to the value of $M(k)$, but the contribution of the $M_2(k)$ is also significant and reduces the result of $M(k)$, especially at large wavenumbers (high energy photoelectrons). Our result of ratio $M_2(k)/M(k)$ obtained is about $-8.01\,\%$ at $k = 10$ Å^{-1}, and $-42.21\,\%$ at $k = 20$ Å^{-1}. The phase difference $\Delta\Phi(k)$, including

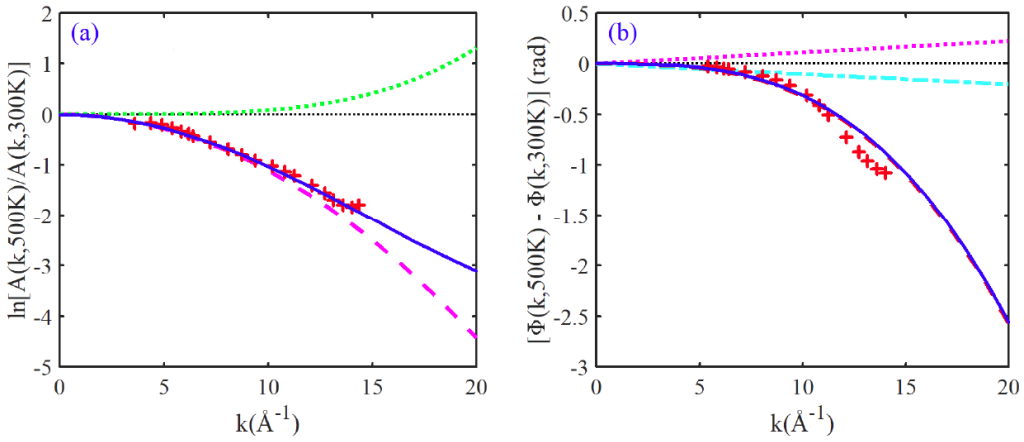

Figure 5: Wavenumber dependence of logarithm of the amplitude ratio (a) and the phase difference (b) of Cu at 500 K and 300 K obtained using the ratio method [49] (red plus signs) and the CACE model in the cases: calculating all of the terms in Eq. (12) or Eq. (13) (solid blue lines) and calculating only the term that contains the second cumulant in Eq. (12) (dashed magenta lines), the fourth cumulant in Eq. (12) (dotted green line), the first cumulant in Eq. (13) (dashed-dotted green line), the second cumulant in Eq. (13) (dashed cyan lines), and the third cumulant in Eq. (13) (dotted magenta line).

the contributions of the terms that contain the first cumulant (henceforth denoted as $\Delta\Phi_1(k)$), the second cumulant (henceforth denoted as $\Delta\Phi_2(k)$), and the third cumulant (henceforth denoted as $\Delta\Phi_3(k)$) as seen via Eq. (13). As can be seen from Figure **5b**, our calculated result demonstrates that the contributions of $\Delta\Phi_1(k)$ and $\Delta\Phi_2(k)$ to the result of $\Delta\Phi(k)$ are significant, but the contribution of $\Delta\Phi_1(k)$ is opposite and only slightly larger than that of $\Delta\Phi_2(k)$, which makes them eliminate each other and causes $\Delta\Phi_3(k)$ to have the most influence on the result of $\Delta\Phi(k)$, especially at large wavenumbers. Our result of ratio $\Delta\Phi_3(k)/\Delta\Phi(k)$ obtained is about $103.08\,\%$ at $k = 10$ Å^{-1} and $100.75\,\%$ at $k = 10$ Å^{-1}.

Consequently, at large wavenumbers, the contribution of $M_2(k)$ cannot be ignored in the calculation of the logarithm of the amplitude ratio $M(k)$, and the approximation $\Delta\Phi(k) \approx \Delta\Phi_3(k)$ can be satisfactory with negligible errors in the calculation of the phase difference $\Delta\Phi(k)$, which means that the term containing the fourth cumulant in Eq. (12) needs to be taken into account, and the terms containing the first and second cumulants can be ignored in Eq. (13) in analyzing the anharmonic EXAFS spectra.

5. CONCLUSIONS

The advantage of the present CACE model compared to other theoretical procedures is that the results of the first four EXAFS cumulants are not only expressed in explicit and simple forms of he temperature *T* or MSRD but also satisfy all of their fundamental properties in temperature dependence. These results are useful not only for numerical calculations and predicting results of other theoretical procedures but also for reducing measurements and analyzing the experimental EXAFS spectra.

The analytical results of the contributions of the EXAFS cumulants to the anharmonic EXAFS oscillation discovered that the third cumulant plays an important role and has the greatest influence on the amplitude reduction, while the fourth cumulant plays an indispensable role and significantly influences on the phase shift, especially at large wavenumbers. This evaluation result is very useful for analyzing the experimental data of the anharmonic EXAFS spectra.

The present method can be applied to the analysis of the anharmonic EXAFS spectra starting from about the correlated Einstein temperature to just before the melting point when the structure of diamond crystals remains stable. In spite of limitations in the application at low temperatures, the present CACE model is still suited to analyze the anharmonic effects in experimental EXAFS spectra, because anharmonicity in EXAFS spectra appears from about room temperature.

The good agreement of our numerical results for Cu with those obtained using the QACE model, ACD model, and other experiments at various temperatures shows the effectiveness of the present CACE model for calculating and analyzing the anharmonic EXAFS spectra.

ACKNOWLEDGEMENTS

This work was supported by the Institute of Research and Development, Duy Tan University, Da Nang 550000, Vietnam.

REFERENCES

[1] Lytle FW, Sayers DE, Stern EA. Phys Rev B 1975; 11: 4825. https://doi.org/10.1103/PhysRevB.11.4825

[2] Beni G, Platzman PM. Phys Rev B 1976; 14: 1514. https://doi.org/10.1103/PhysRevB.14.1514

[3] Eisenberger P, Brown GS. Solid State Commun 1979; 29: 481. https://doi.org/10.1016/0038-1098(79)90790-7

[4] Greegor RB, Lytle FW. Phys Rev B 1979; 20: 4902. https://doi.org/10.1103/PhysRevB.20.4902

[5] Stern EA, Bunker BA, Heald SM. Phys Rev B 1980; 21: 5521. https://doi.org/10.1103/PhysRevB.21.5521

[6] Lee PA, Citrin PH, Eisenberger P, Kincaid BM. Rev Mod Phys 1981; 53: 769. https://doi.org/10.1103/RevModPhys.53.769

[7] Bunker G. Nucl Instrum Methods 1983; 207: 437. https://doi.org/10.1016/0167-5087(83)90655-5

[8] Rehr JJ, Albers RC. Rev Mod Phys 2000; 72: 621. https://doi.org/10.1103/RevModPhys.72.621

[9] Tranquada JM, Ingalls R. Phys Rev B 1983; 28: 3520. https://doi.org/10.1103/PhysRevB.28.3520

[10] Crozier ED, Rehr JJ, Ingalls R. X-ray Absorption: Principles, Applications, Techniques of EXAFS, SEXAFS and XANES, edited by D.C. Koningsberger & R. Prins (John Wiley & Sons, New York), 1988; Chap. 9.

[11] Hung NV, Hung LH, Tien TS, Frahm RR. Int J Mod Phys B 2008; 22: 5155. https://doi.org/10.1142/S0217979208049285

[12] Hung NV, Fornasini P. J Phys Soc Jpn 2007; 76: 084601. https://doi.org/10.1143/JPSJ.76.084601

[13] Hung NV, Thang CS, Duc NB, Vuong DQ, Tien TS. Physica B 2017; 521: 198. https://doi.org/10.1016/j.physb.2017.06.027

[14] Hung NV, Thang CS, Duc NB, Vuong DQ, Tien TS. Eur Phys J B 2017; 90: 256. https://doi.org/10.1140/epjb/e2017-80383-1

[15] Hung NV, Duc NB, Vuong DQ, Toan NC, Tien TS. Vacuum 2019; 169: 108872. https://doi.org/10.1016/j.vacuum.2019.108872

[16] Fornasini P, Grisenti R, Dapiaggi M, Agostini G, Miyanaga T. J Chem Phys 2017; 147: 044503. https://doi.org/10.1063/1.4995435

[17] Kubo R. J Phys Soc Jpn 1962; 17: 1100. https://doi.org/10.1143/JPSJ.17.1100

[18] Hung NV, Rehr JJ. Phys Rev B 1997; 56: 43. https://doi.org/10.1103/PhysRevB.56.43

[19] Tröger L, Yokoyama T, Arvanitis D, Lederer T, Tischer M, Baberschke K. Phys Rev B 1994; 49: 888. https://doi.org/10.1103/PhysRevB.49.888

[20] Dalba G, Fornasini P, Grazioli M. Phys Rev B 1995; 76: 11034. https://doi.org/10.1103/PhysRevB.52.11034

[21] Dalba G, Fornasini P. J Synchrotron Radiat 1997; 4: 243. https://doi.org/10.1107/S0909049597006900

[22] Dalba G, Fornasini P, Grisenti R, Pasqualini D, Diop D, Monti F. Phys Rev B 1998; 58: 4793. https://doi.org/10.1103/PhysRevB.58.4793

[23] Yokoyama T, Ohta T, Sato H. Phys Rev B 1997; 55: 11329. https://doi.org/10.1103/PhysRevB.55.11320

[24] Soldo Y, Hazemann JL, Aberdam D, Inui M, Tamura K, Raoux D, Pernot E, Jal JF, Philon JD. Phys Rev B 1998; 57: 258. https://doi.org/10.1103/PhysRevB.57.258

[25] Bus E, Miller JT, Kropf AJ, Prins R, Bokhoven JAV. Phys Chem Chem Phys 2006; 8: 3248. https://doi.org/10.1039/b605248g

[26] Vaccari M, Grisenti R, Fornasini P, Rocca F, Sanson A. Phys Rev B 2007; 75: 184307. https://doi.org/10.1103/PhysRevB.75.184307

[27] Ahmed SI, Dalba G, Fornasini P, Vaccari M, Rocca F, Sanson A, Li J, Sleight AW. Phys Rev B 2009; 79: 104302. https://doi.org/10.1103/PhysRevB.79.104302

[28] Miyanaga T, Fujikawa T. J Phys Soc Jpn 1994; 63: 3683. https://doi.org/10.1143/JPSJ.63.3683

[29] Yokoyama T. Phys Rev B 1998; 57: 3423. https://doi.org/10.1103/PhysRevB.57.3423

[30] Yokoyama T. J Synchrotron Radiat 1999; 6: 323. https://doi.org/10.1107/S0909049599001521

[31] Poiarkova AV, Rehr JJ. Phys Rev B 1999; 59: 948. https://doi.org/10.1103/PhysRevB.59.948

[32] Beccara SA, Dalba G, Fornasini P, Grisenti R, Pederiva F, Sanson A, Diop D, Rocca F. Phys Rev B 2003; 68: 140301. https://doi.org/10.1103/PhysRevB.68.140301

[33] Beccara SA, Fornasini P. Phys Rev B 2008; 77: 172304. https://doi.org/10.1103/PhysRevB.77.172304

[34] Vila FD, Rehr JJ, Rossner HH, Krappe HJ. Phys Rev B 2007; 76: 014301. https://doi.org/10.1103/PhysRevB.76.014301

[35] Vila FD, Lindahl VE, Rehr JJ. Phys Rev B 2012; 85: 024303. https://doi.org/10.1103/PhysRevB.85.024303

[36] Hung NV, Trung NB, Kirchner B. Physica B 2010; 405: 2519. https://doi.org/10.1016/j.physb.2010.03.013

[37] Stern EA, Livins P, Zhang Z. Phys Rev B 1991; 43: 8850. https://doi.org/10.1103/PhysRevB.43.8850

[38] Pirog IV, Nedoseikina TI, Zarubin IA, Shuvaev AT. J Phys Condens Matter 2002; 14: 1825. https://doi.org/10.1088/0953-8984/14/8/311

[39] Pirog IV, Nedoseikina TI. Physica B 2003; 334: 123. https://doi.org/10.1016/S0921-4526(03)00034-6

[40] Vlasenko VG, Podsukhina SS, Kozinkin AV, Zubavichus YaV. Phys Solid State 2016; 58: 421. https://doi.org/10.1134/S1063783416020335

[41] Frenkel AI, Rehr JJ. Phys Rev B 1993; 48: 585. https://doi.org/10.1103/PhysRevB.48.585

[42] Miyanaga T, Fujikawa T. J Phys Soc Jpn 1994; 63: 1036. https://doi.org/10.1143/JPSJ.63.1036

[43] Hung NV, Tien TS, Duc NB, Vuong DQ. Mod Phys Lett B 2014; 28: 1450174. https://doi.org/10.1142/S0217984914501747

[44] Tien TS, Hung NV, Tuan NT, Nam NV, An NQ, Thuy NTM, Lien VTK, Nghia NV. J Phys Chem Solids 2019; 134: 307. https://doi.org/10.1016/j.jpcs.2019.06.020

[45] Rehr JJ, Zabinsky SI, Ankudinov A, Albers RC. Physica B 1995; 208 & 209: 23. https://doi.org/10.1016/0921-4526(94)00623-4

[46] Sevillano E, Meuth H, Rehr JJ. Phys Rev B 1979; 20: 4908. https://doi.org/10.1103/PhysRevB.20.4908

[47] Duc NB, Tho NQ. Physica B 2019; 552: 1. https://doi.org/10.1016/j.physb.2018.09.038

[48] Vuong DQ, Hung NV. J Mod Phys Lett B 2019; 33: 1950078. https://doi.org/10.1142/S0217984919500787

[49] Fornasini P, Beccara SA, Dalba G, Grisenti R, Sanson A, Vaccari M, Rocca F. Phys Rev B 2004; 70: 174301. https://doi.org/10.1103/PhysRevB.70.174301

[50] Yokoyama T, Kobayashi K, Ohta T, Ugawa A. Phys Rev B 1996; 53: 6111. https://doi.org/10.1103/PhysRevB.53.6111

[51] Freund J, Ingalls R, Crozier ED. Phys Rev 1989; 39: 12537. https://doi.org/10.1103/PhysRevB.39.12537

[52] Comaschi T, Balerna A, Mobilio S. J Phys Condens Matter 2009; 21: 325404. https://doi.org/10.1088/0953-8984/21/32/325404

[53] Dalba G, Fornasini P, Rocca E. Phys Rev B 1993; 47: 8502. https://doi.org/10.1103/PhysRevB.47.8502

[54] Morse PM. Phys Rev 1929; 34: 57. https://doi.org/10.1103/PhysRev.34.57

[55] Girifalco LA, Weizer VG. Phys Rev 1959; 114: 687. https://doi.org/10.1103/PhysRev.114.687

Received on 28-11-2019 Accepted on 14-12-2019 Published on 23-12-2019

DOI: https://doi.org/10.31875/2410-4701.2019.06.15